Protein Structure and Folding:

Structure of eIF3b RNA Recognition Motif and Its Interaction with eIF3j: STRUCTURAL INSIGHTS INTO THE RECRUITMENT OF eIF3b TO THE 40 S RIBOSOMAL SUBUNIT

Latifa ElAntak, Andreas G. Tzakos, Nicolas Locker and Peter J. Lukavsky

J. Biol. Chem. 2007, 282:8165-8174.
doi: 10.1074/jbc.M610860200 originally published online December 26, 2006

THE JOURNAL OF BIOLOGICAL CHEMISTRY VOL. 282, NO. 11, pp. 8165–8174, March 16, 2007

Structure of eIF3b RNA Recognition Motif and Its Interaction with eIF3j

STRUCTURAL INSIGHTS INTO THE RECRUITMENT OF eIF3b TO THE 40 S RIBOSOMAL SUBUNIT[*] [S]

Received for publication, November 24, 2006, and in revised form, December 18, 2006 Published, JBC Papers in Press, December 26, 2006, DOI 10.1074/jbc.M610860200

Latifa ElAntak[1], **Andreas G. Tzakos**[2], **Nicolas Locker**[1], **and Peter J. Lukavsky**[3]

From the Laboratory of Molecular Biology, Medical Research Council, Hills Road, Cambridge CB2 2QH, United Kingdom

Mammalian eIF3 is a 700-kDa multiprotein complex essential for initiation of protein synthesis in eukaryotic cells. It consists of 13 subunits (eIF3a to -m), among which eIF3b serves as a major scaffolding protein. Here we report the solution structure of the N-terminal RNA recognition motif of human eIF3b (eIF3b-RRM) determined by NMR spectroscopy. The structure reveals a noncanonical RRM with a negatively charged surface in the β-sheet area contradictory with potential RNA binding activity. Instead, eIF3j, which is required for stable 40 S ribosome binding of the eIF3 complex, specifically binds to the rear α-helices of the eIF3b-RRM, opposite to its β-sheet surface. Moreover, we identify that an N-terminal 69-amino acid peptide of eIF3j is sufficient for binding to eIF3b-RRM and that this interaction is essential for eIF3b-RRM recruitment to the 40 S ribosomal subunit. Our results provide the first structure of an important subdomain of a core eIF3 subunit and detailed insights into protein-protein interactions between two eIF3 subunits required for stable eIF3 recruitment to the 40 S subunit.

Protein synthesis is crucial for the survival and propagation of life and represents one of the most complex and central events in the life cycle of eukaryotic cells. The initiation phase of protein synthesis requires at least 12 eukaryotic initiation factors (eIFs)[4] to assemble 80 S ribosomes onto mRNA with the anticodon of $tRNA_i^{Met}$ base-paired to the authentic AUG start codon (for a review, see Ref. 1). Among these eIFs, eIF3 is the most complex initiation factor, comprising 13 polypeptide subunits (a–m) in mammalian cells with a total molecular mass of ~700 kDa (2). The eIF3 complex plays an essential role both in cellular and viral initiation of translation through its direct binding to the 40 S ribosomal subunit, other eIFs, and mRNAs bearing either a 5′-cap, or an internal ribosome entry site (1). eIF3 stimulates eIF2·GTP·$tRNA_i^{Met}$ ternary complex binding to 40 S subunits and aids correct positioning of mRNAs within 48 S initiation complexes (for a review, see Ref. 3). In addition, eIF3 is involved in the dissociation of 80 S ribosomes from mRNA after termination of translation and serves as an anti-association factor preventing 60 S subunit binding to 40 S subunits prior to the subsequent 48 S initiation complex formation (4, 5). The recent cryoelectron microscopy structure of free human eIF3 revealed an overall five-lobed architecture particle (6). Its interaction with 40 S subunit was modeled, and it has been suggested that eIF3 could be located on the solvent-exposed side of the 40 S particle (6). The activity of eIF3 must rely on the organization of the individual eIF3 subunits within that overall five-lobed architecture; however, no details of the spatial arrangement of the subunits and the interactions between them have been established.

Among the components of eIF3, eIF3b is considered to be the major scaffolding subunit within the eIF3 complex, interacting with eIF3a (7), eIF3g, eIF3i, and eIF3j (8). The yeast homologue of the eIF3b subunit, PRT1, interacts with the yeast homologues of eIF3a (TIF32), eIF3g (TIF35), eIF3i (TIF34), eIF3j (HCR1), and eIF3e (Pci8) (9–11), highlighting the conserved role of eIF3b in the structural organization of the eIF3 complex. The human eIF3b subunit is an 814-amino acid protein, whose primary sequence reveals only one identifiable domain, an RNA recognition motif (RRM), located in its N terminus (7). The RRM is a widespread structural motif with a conserved protein fold composed of a four-stranded antiparallel β-sheet packed against two α-helices (βαββαβ fold). At the sequence level, the canonical RRM is characterized by two conserved ribonucleoprotein (RNP) sequences, RNP1 and RNP2, both of which contain conserved aromatic residues essential for RNA binding (12, 13). Interestingly, the eIF3b-RRM sequence (see supplemental Fig. S1) is devoid of any aromatic residues in the RNP2, which is atypical for a classical RRM.

In yeast, eIF3b (PRT1) also contains an N-terminal RRM, which is crucial for the integrity of the eIF3 complex and important for 40 S subunit binding (10). Both yeast homologues of eIF3a (TIF32) and eIF3j (HCR1) have been shown to interact directly with PRT1-RRM (10). Removal of the RRM from PRT1 (eIF3b) disrupts the interaction with TIF32 (eIF3a) and HCR1 (eIF3j) and abolishes 40 S subunit binding of the remaining eIF3 subcomplexes (10). The HCR1 subunit binds to both 40 S sub-

[*] The costs of publication of this article were defrayed in part by the payment of page charges. This article must therefore be hereby marked "*advertisement*" in accordance with 18 U.S.C. Section 1734 solely to indicate this fact.

[S] The on-line version of this article (available at http://www.jbc.org) contains supplemental Figs. S1–S4.

The atomic coordinates and structure factors (code 2NLW) have been deposited in the Protein Data Bank, Research Collaboratory for Structural Bioinformatics, Rutgers University, New Brunswick, NJ (http://www.rcsb.org/).

[1] Medical Research Council career development fellow.

[2] European Molecular Biology Organization long term fellow.

[3] To whom correspondence should be addressed: Medical Research Council-Laboratory of Molecular Biology, Structural Studies Division. Tel.: 44-1223-402417; Fax: 44-1223-213556; E-mail: pjl@mrc-lmb.cam.ac.uk.

[4] The abbreviations used are: eIF, eukaryotic initiation factor; RRM, RNA recognition motif; RNP, ribonucleoprotein; NOE, nuclear Overhauser effect; NOESY, NOE spectroscopy; ITC, isothermal titration calorimetry; UHM, U2AF homology motif.

units and the PRT1-RRM, which stimulates binding of the eIF3 complex to 40 S subunits (10). In humans, eIF3j is also required for stable 40 S ribosome binding to the eIF3 complex; eIF3 lacking eIF3j binds only weakly to 40 S subunits, but tight binding can be restored *in vitro* upon the addition of eIF3j (8). All of these data indicate that the interaction between eIF3b and eIF3j is crucial for the eIF3 recruitment to the 40 S ribosome. To date, however, there are no detailed structural data on these eIF3 subunits and their interactions.

In the present study, we report the solution structure of the RRM domain from human eIF3b determined by NMR spectroscopy. The eIF3b-RRM shows characteristic structural features of a noncanonical RRM and, in addition, a highly negatively charged surface within the β-sheet area contradictory to potential RNA binding. We demonstrate that the eIF3b-RRM, instead, interacts directly with the eIF3j subunit. We have identified the detailed interaction interface on the eIF3b-RRM as well as the eIF3j subdomain for the interaction. In addition, we show that binding of eIF3b-RRM to 40 S ribosomal subunits is only established in the presence of intact eIF3j, suggesting that eIF3j might serve as a bridging molecule between eIF3b-RRM and the 40 S subunit. Our results give the first detailed structural insights of essential protein-protein interactions within the eIF3 complex.

EXPERIMENTAL PROCEDURES

Preparation of Recombinant Proteins—A DNA fragment encoding the eIF3b-RRM (residues 170–274 of the human eIF3b subunit) was prepared by PCR from cDNA libraries (Clontech) and subcloned into pET28a vector (Novagen). The protein was expressed in *Escherichia coli* BL21(DE3) as an N-terminal His_6 tag fusion. ^{15}N-Labeled and ^{15}N-^{13}C-labeled proteins were obtained by expressing eIF3b-RRM in M9 minimal medium supplemented with $^{15}NH_4Cl$ or $^{15}NH_4Cl$ and [^{13}C]glucose, respectively. Protein expression was induced by the addition of 1 mM isopropyl 1-thio-β-D-galactopyranoside and further incubation for 3 h at 37 °C. The purification of the His_6-eIF3b-RRM was performed on a HiTrap chelating column (Amersham Biosciences) charged with nickel sulfate under standard conditions. After tobacco etch virus protease cleavage to remove free His_6 tag, the reaction mixture was loaded on a HiTrap chelating column charged with nickel sulfate to remove all of the tobacco etch virus protease (His_6-tagged) as well as minor contaminating proteins, which co-purified with His_6-eIF3b-RRM during the first HiTrap chelating column. After the second HiTrap chelating column, the eIF3b-RRM was pure on SDS-polyacrylamide gel with no visible contaminants. The protein was then equilibrated against appropriate buffer for further experiments using Vivaspin 2 centrifugal devices (Sartorius).

A DNA fragment encoding the eIF3j subunit with a deletion of 6 of 7 nonconserved N-terminal alanine residues to eliminate the GC-rich coding sequence and enable preparation by PCR from cDNA libraries (Clontech), was subcloned into pET28a vector (Novagen) as His_6-tagged fusion protein. The latter plasmid was used to prepare DNA fragments encoding the eIF3j deletion mutants (Δ16C-eIF3j, Δ80C-eIF3j, Δ69N-eIF3j, and 69N-eIF3j) by PCR with appropriate primers and subcloned into pET28a vector as His_6-tagged fusion proteins. All eIF3j proteins were expressed and purified as described above.

NMR Experiments—The NMR experiments were carried out at 298 K on Bruker AMX500 or AVANCE-800 spectrometers equipped with cryoprobes and on a Bruker DMX600 spectrometer. The NMR spectra were processed using XWINNMR (Bruker) and analyzed using the Sparky program (14). The NMR samples contained 0.8 mM eIF3b-RRM in 20 mM Hepes (pH 7.5), 0.3 M NaCl, 10% D_2O. The backbone resonances of eIF3b-RRM were assigned using standard three-dimensional HNCA, HN(CO)CA, CBCA(CO)NH, CBCANH, HBHA(CO)NH, and HBHANH. The aliphatic and aromatic side chain resonances were assigned using three-dimensional HCCH-TOCSY, three-dimensional ^1H,^{15}N,^1H NOESY, and two-dimensional NOESY experiments. NOE distance restraints were obtained from homonuclear two-dimensional NOESY and three-dimensional ^1H,^{15}N,^1H NOESY data. Angular restraints (ϕ and ψ) were obtained from chemical shift values of N, Hα, Cα, and Cβ resonances by using the TALOS program (15).

Structure Calculations—The three-dimensional protein structures were calculated with the program CYANA (16), using automated long range NOE assignment and TALOS angle restraints (15). A standard torsion angle dynamics protocol has been used for the structure calculation using 100 starting structures with random torsion angle values together with 1336 NOE-based distance as well as 151 φ and ψ dihedral angle restraints. Appropriate conversions of structure and restraint parameter files were achieved by the utilization of FormatConverter (17). The final set of structures was obtained from water refinement calculations in CNS (18), using the standard RECOORD protocols (19). The 16 lowest energy conformers were selected to represent the ensemble structure, and the lowest energy conformer was used for all of the figures. The quality of the ensemble of structures was evaluated by the PROCHECK program (20).

NMR Titration Experiments—Titration experiments were carried out in 20 mM Hepes (pH 7.5), 0.1 M NaCl, 10% D_2O as follows: 0.1 mM, 0.2 mM, and 0.4 mM final concentration of unlabeled eIF3j or eIF3j deletion mutants (0.5, 1, and 2 eq) were added to 0.2 mM ^{15}N-labeled eIF3b-RRM. Chemical shift perturbations in the eIF3b-RRM were monitored in two-dimensional ^1H-^{15}N HSQC experiments. Weighted average chemical shift variations were calculated according to the formula, $\Delta ppm = ((\Delta\delta_{HN})^2 + (\Delta\delta_N \times 0.17)^2)1/2$. To estimate the dependence of salt in the complex formation, the experiments were also carried out with protein samples in buffer containing 0.4 M NaCl.

Gel Mobility Shift Assays—Purified eIF3j (30 μM final concentration) was incubated with increasing amount of purified eIF3b-RRM (7.5, 15, 22.5, 30, or 60 μM final concentration) in a final volume of 20 μl containing 10 mM Tris-HCl buffer (pH 7.4) and 50 mM NaCl.Complexes were formed at room temperature and analyzed on 8% native polyacrylamide gels. Gel electrophoresis was performed for 1 h at 100 V at 4 °C using Tris-glycine running buffer. Proteins were visualized using SimplyBlue™ SafeStain (Invitrogen).

Isothermal Titration Calorimetry Measurements—Titration calorimetry measurements were performed on a Microcal VP titration calorimeter. The protein solutions were prepared in 20

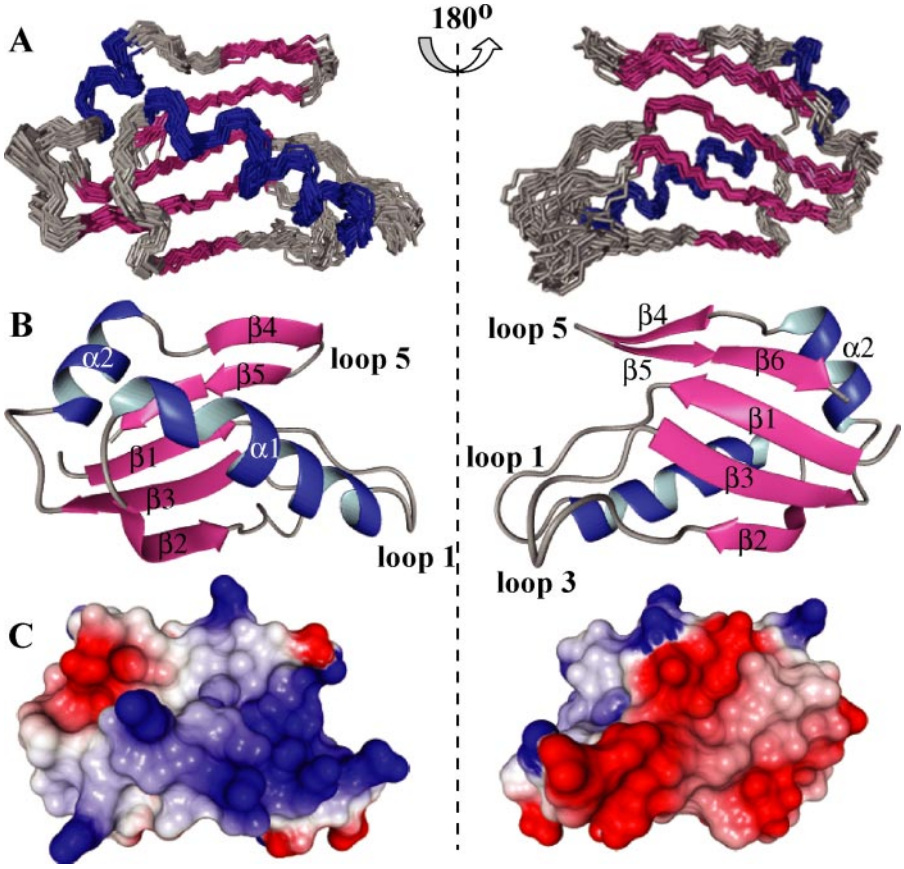

FIGURE 1. **Solution structure of the human eIF3b-RRM (residues 185–264 are displayed).** *A*, ensemble of the backbone traces of the 16 lowest energy conformers of eIF3b-RRM. *B*, *ribbon diagram* of the eIF3b-RRM structure. The secondary structure elements are *numbered*. *C*, electrostatic surface potential of the eIF3b-RRM in the same orientation as in *B*. Electronegative (acidic) regions are *colored red*, and electropositive (basic) regions are *colored blue*. The structures are displayed using MOLMOL (40).

mM Hepes buffer (pH 7.5), 0.15 M NaCl at a concentration of 1 mM for eIF3b-RRM and 50 μM for eIF3j samples, respectively. All of the experiments were performed at 25 °C. 7-μl aliquots of eIF3b-RRM solution were injected into an eIF3j solution every 210 s, during which the titration peak returned to the base line. Four extra injections were made at the end of each run (after saturation) to measure the heat of dilution. The titration data were analyzed using the ORIGIN software to obtain thermodynamic parameters.

His_6 Tag Pull-down Assays—His_6-tagged eIF3b-RRM and untagged eIF3j deletion mutants were prepared as described above and buffer-exchanged in equilibration buffer (50 mM sodium phosphate, pH 8, 0.1 M NaCl). His_6-eIF3b-RRM was incubated with each of the unlabeled eIF3j mutant for 15 min at room temperature and loaded on His-select spin columns (Sigma) equilibrated with equilibration buffer. After two washing steps with equilibration buffer containing 5 mM imidazole, proteins were eluted with elution buffer (50 mM sodium phosphate pH 8, 0.1 M NaCl, 250 mM imidazole). The eluted proteins were resolved by denaturating gel electrophoresis and visualized by staining with SimplyBlue™ SafeStain (Invitrogen).

40 S Ribosomal Subunit Binding Assays—^{35}S-Labeled eIF3b-RRM and eIF3j were prepared using the TnT coupled rabbit reticulocyte *in vitro* translation and transcription system (Promega). Both proteins were synthesized by incubating 1 μg of plasmid in 40 μl of TnT Quick Master mixture with 2 μl of L-[^{35}S]methionine (Amersham Biosciences) for 90 min at 30 °C. The *in vitro* translated products were then purified using HIS-Select™ spin columns (Sigma) according to the manufacturer's instructions. Unlabeled eIF3j and Δ69N-eIF3j were expressed in *E. coli* and purified as above.

40 S subunits were prepared according to a previously published protocol (21). Assembly of ribosomal complexes used 1–2 pmol of ^{35}S-labeled or unlabeled eIF3b-RRM, eIF3j or Δ69N-eIF3j and 10 pmol of 40 S subunits in 20 μl of buffer X (20 mM Tris-HCl, pH 7.6, 100 mM KCl, 2 mM $MgOAc_2$, 2 mM dithiothreitol) at 37 °C for 5 min. The reaction mixtures were loaded and resolved on a 1% native agarose gel prepared with buffer X. Gel electrophoresis was performed for 1 h at 100 V at 4 °C using buffer X as running buffer. Gels were then dried on Whatman paper and exposed overnight on a PhosphorImager screen.

RESULTS

Structure of Human eIF3b-RRM Reveals Characteristics of a Noncanonical RRM—A fragment of eIF3b spanning residues 170–274 (eIF3b-RRM; see supplemental Fig. S1), including the RRM domain (residues 185–268), was overexpressed, isotopically labeled, and purified. The solution structure determination of the eIF3b-RRM employed standard homo- and heteronuclear NMR techniques. The ^{1}H-^{15}N HSQC spectrum displays a very good chemical shift dispersion, indicating a well folded protein domain. Standard triple resonance experiments were used to assign the chemical shifts of the protein enabling the assignment of more than 99% of the backbone resonances and 96% of the side chain resonances. Using 1336 NOE distances and 151 TALOS-derived angle restraints (15), 100 structures were calculated. The final 16 lowest energy structures are shown in Fig. 1*A*. These conformers have an average backbone root mean square deviation of 0.53 Å for the secondary structure elements, and they present no distance violations over 0.35 Å or angle violations larger than 5°. The quality of the structures was evaluated using the PROCHECK software (20) and showed good statistics in the backbone ϕ-ψ angle distribution. The statistical analysis of the eIF3b-RRM structure is reported in Table 1.

The eIF3b-RRM adopts an overall RRM fold (Fig. 1*B*). The four-stranded antiparallel β-sheet is constituted by strands β1 (residues 186–190), β2 (217–221), β3 (232–237), and β6 (262–264). Two α-helices, α1 (residues 200–213) and α2 (residues 242–249), are perpendicular to each other and packed on one

TABLE 1
Structural statistics of the eIF3b-RRM calculated structures

Parameter	Value
No. of distance constraints	
All	1336
Intraresidual	380
Sequential ($\|i-j\|=1$)	419
Medium ($1<\|i-j\|\leq 4$)	216
Long ($\|i-j\|>4$)	321
No. of dihedral angle restraints (backbone φ and ψ)	151
Restraint violations	
Distance restraints violated by >0.35 Å	0
Torsion angle restrains violated by >5 Å	0
Root mean square deviation against the mean structure	
Backbone (secondary structure regions) (Å)	0.53 ± 0.08
Heavy (secondary structure regions) (Å)	1.08 ± 0.07
Root mean square deviation from ideal covalent geometry	
Bonds (Å)	0.018 ± 0.00053
Angles (degrees)	1.415 ± 0.0308
Improper torsion angles (degrees)	1.915 ± 0.1713
Ramachandran analysis	
Residues in most favorable regions (%)	81.3
Residues in additional allowed regions (%)	15.6
Residues in generously allowed regions (%)	2.2
Residues in disallowed regions (%)	0.9

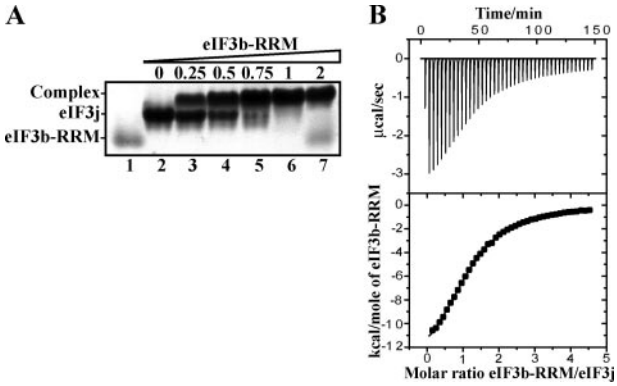

FIGURE 2. *A*, the human eIF3b-RRM interacts with eIF3j. Gel mobility shift assays performed with 30 μM purified human eIF3j subunit in the absence (*lane 2*) and in the presence of increasing amount (*lanes 3*-7) of purified human eIF3b-RRM (7.5, 15, 22.5, 30, and 60 μM). The *numbers above* indicate the *x*-fold molar excess of eIF3b-RRM over eIF3j. *B*, isothermal calorimetric titration of eIF3j with eIF3b-RRM. The *upper panel* shows raw data of heat effect (in μcal·s^{-1}) of 7-μl injections of 1 mM eIF3b-RRM into 1.5 ml of 50 μM eIF3j performed at 210-s intervals. The *lower panel* shows the fitted binding isotherms. The data points were obtained by integration of heat signals plotted against the molar ratio of eIF3b-RRM to eIF3j in the reaction cell. The *solid line* represents a calculated curve using the best fit parameters obtained by a nonlinear least squares fit.

side of the β-sheet. The eIF3b-RRM structure also presents three larger loops: loop 1 between β1 and α1 (residues 191–199), loop 3 between β2 and β3 (residues 222–231), and loop 5 between α2 and β6 (residues 250–261), which forms a β-hairpin involving strands β4 (residues 253–256) and β5 (residues 259–261). This β-hairpin is not an essential structural determinant of the RRM fold; however, it has been observed in other RRMs (22, 23). The eIF3b-RRM also displays a particularly extended helix α1, comprising 14 amino acids (Fig. 1). This helix does not exceed 10 amino acids in canonical RRMs. The N- and C-terminal regions flanking the RRM (residues 170–182 and 268–274, respectively) present flexibility.

The overall structural features of eIF3b-RRM (*i.e.* the absence of aromatic residues in RNP2 and the extended helix α1) are specific characteristics of noncanonical RRMs, which are involved in protein-protein interactions (24). In addition, the structure of eIF3b-RRM displays a highly negatively charged area surrounding the two RNP sequences (Fig. 1*C*). RNA binding to the canonical RRM is usually mediated through stacking interactions between RNA bases and the aromatic side chains from RNP sequences, generally surrounded by basic and polar residues for additional contacts with RNA. In contrast, the eIF3b-RRM lacks aromatic residues in RNP2, and both RNPs are embedded in a cluster of acidic residues, which makes RNA binding to the eIF3b-RRM rather unfavorable. The only positively charged region of the eIF3b-RRM is found on the opposite side of the negatively charged β-sheet surface and comprises the extended helix α1 and the β-hairpin loop 5 (Fig. 1*C*).

Human eIF3j Binds eIF3b-RRM—The eIF3b-RRM displays structural features that are clearly contradictory to a potential role in RNA binding. We therefore decided to investigate the interaction with its candidate protein-binding partner, the eIF3j subunit. Human eIF3j is a 35-kDa protein and is essential for the stable recruitment of the eIF3 complex to 40 S subunits (8). Recombinant eIF3j was expressed in *E. coli* and purified.

In yeast, it has been shown that the homologues of eIF3b (PRT1) and eIF3j (HCR1) interact directly through PRT1-RRM (10). Although co-purification of human eIF3j with full-length eIF3b has been previously reported (8), there is no direct evidence that the RRM domain of human eIF3b provides the interaction surface for eIF3j binding. To test this potential direct interaction, we performed gel mobility shift assays (Fig. 2*A*). The formation of a complex between the two proteins is observed by the appearance of a higher molecular weight band on the native gel (Fig. 2*A*, *lanes 3–7*). At a 1:1 stoichiometry, only the higher molecular weight band is detected (Fig. 2*A*, *lane 6*). The addition of excess eIF3b-RRM leaves unbound eIF3b-RRM (Fig. 2*A*, *lane 7*). Therefore, this indicates that human eIF3b-RRM and eIF3j interact directly at an apparent 1:1 stoichiometry.

To further characterize the formation of the eIF3b-RRM·eIF3j complex, the thermodynamic parameters were obtained from isothermal titration calorimetry (ITC) measurements (Fig. 2*B*). The raw ITC data are shown in the *upper panel* of Fig. 2*B*, and the integrated areas under each peak as a function of molar ratio of eIF3b-RRM to eIF3j are plotted in the *lower panel*. The interaction is characterized by a large negative enthalpy change ($\Delta H = -14.9 \pm 0.1$ kcal/mol), indicating that it is predominantly mediated through charge-charge interactions (25). The binding curve is sigmoidal and best fitted to a single binding site model with ~1:1 stoichiometry, yielding a dissociation constant (K_d) of 20.3 ± 0.4 μM.

Human eIF3b-RRM Interacts with eIF3j via Its Positively Charged Surface—In order to identify the residues of the eIF3b-RRM involved in the interaction with eIF3j, we performed NMR titration experiments. Chemical shift variations were monitored using two-dimensional ^{1}H-^{15}N HSQC spectra (see supplemental Fig. S2). Specific chemical shift perturbations were observed upon the addition of increasing amounts of unlabeled eIF3j to ^{15}N-labeled eIF3b-RRM, indicative of an equilibrium between the bound and unbound states in the fast

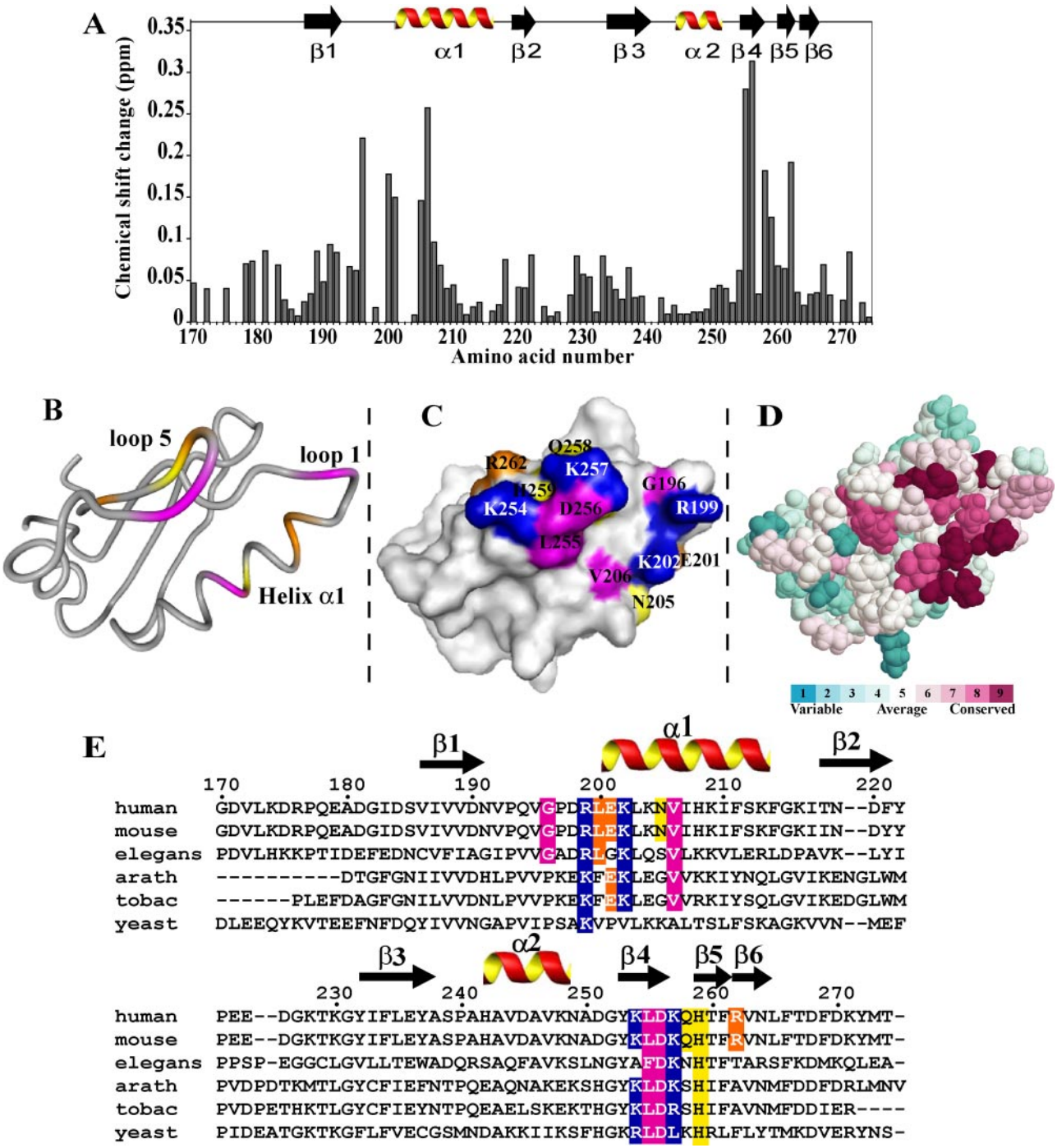

FIGURE 3. **Mapping eIF3b-RRM/eIF3j interaction site by heteronuclear NMR.** *A*, plot of the weighted average chemical shift variations of ^{15}N-eIF3b-RRM backbone upon the addition of eIF3j. The amide resonances of five residues (Lys^{174}, Arg^{199}, Lys^{202}, Leu^{203}, and Phe^{269}) could not be unambiguously assigned in the bound spectra. Secondary structures of eIF3b-RRM are shown *above* the plot. *B*, chemical shift mapping onto *ribbon representations* of eIF3b-RRM. Residues are *colored* based on the magnitude of shift changes upon eIF3j binding. The *color code* is as follows. *Magenta*, Δ_{avg}(HN) $>$ 0.2 ppm; *orange*, 0.2 $<$ Δ_{avg}(HN) $<$ 0.15 ppm; *yellow*, 0.15 $<$ Δ_{avg}(HN) $<$ 0.1 ppm; *white*, not observed or could not be measured. *C*, surface representation of the data presented in *B*, with the interacting residues labeled. In addition, conserved basic residues close to the interacting residues are highlighted in *blue* (opposite representation of the interacting surface shown in supplemental Fig. S3). *D*, eIF3b RRM is presented also using a space-filled model. The amino acids are *colored* by their conservation grades using the *color coding bar*, with *turquoise* through *maroon* indicating variable through conserved. The run was carried out using the Protein Data Bank structure of elf3b RRM, sequence alignment of the eIF3b-RRM from different species, and default ConSurf parameters. The picture was generated using Rasmol. *B–D*, the same orientation of the eIF3b-RRM molecule is used. *E*, sequence alignment of eIF3b-RRM from different organisms (humans (this study), mice, *Caenorhabditis elegans* (*elegans*), *Arabidopsis thaliana* (*arath*), *Nicotiana tabacum* (*tobac*), and yeast). Conserved residues that mediate recognition of eIF3j by eIF3b-RRM are shown according to the *color code* described in *B* and *C*. Secondary structures of eIF3b-RRM are shown *above* the sequence.

exchange regime. The NMR spectra remained unchanged beyond the equimolar addition of eIF3j, confirming the formation of a complex with 1:1 stoichiometry. The weighted average chemical shift displacements are shown in Fig. 3*A*. The largest chemical shift variations between the free and the bound forms of eIF3b-RRM are observed for backbone amides of loop 1

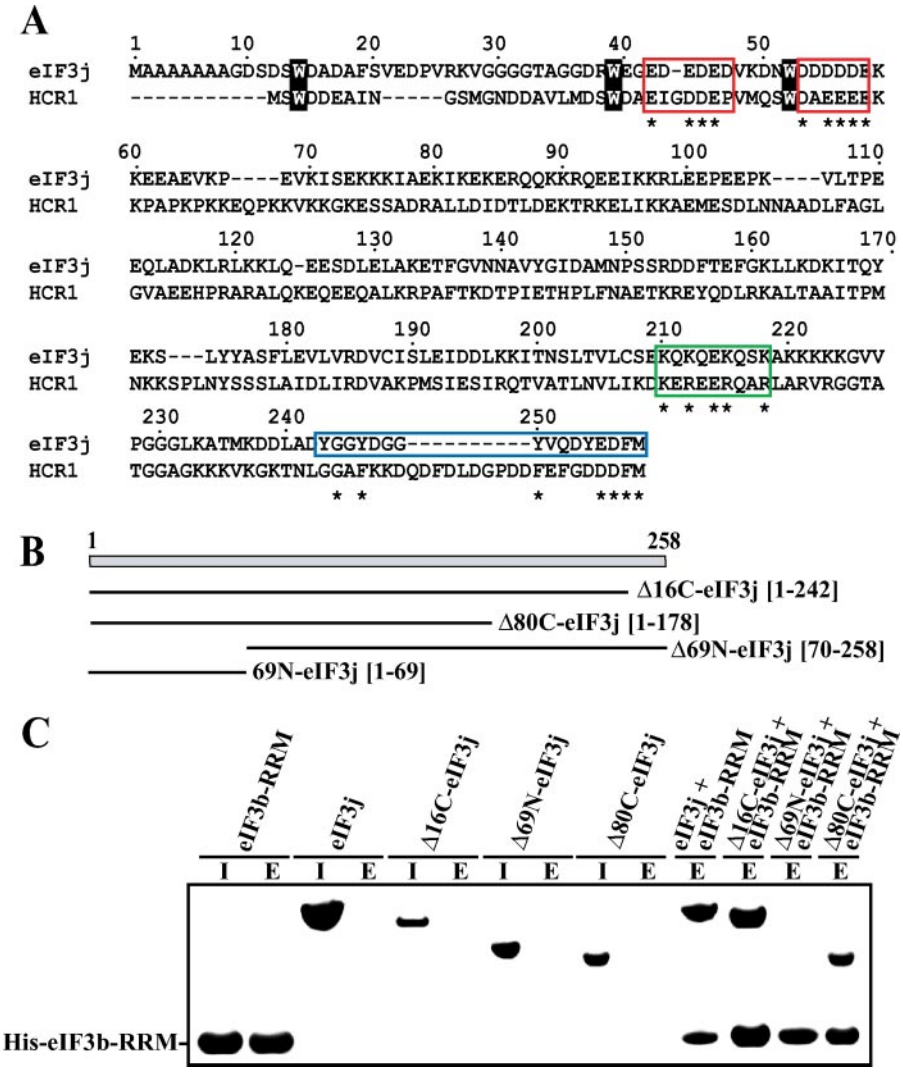

FIGURE 4. *A*, sequence alignment of human (*eIF3j*) and yeast eIF3j (*HCR1*). Conserved tryptophan residues are *highlighted white* on *black*. In *red* are *boxed* the N-terminal acidic clusters of the protein. The residues *boxed* in *green* correspond to the conserved motif KX_3EKX_2K (residues 210–218) similar to the KX_5ERX_2R found in HCR1 (10). The 16 last residues involved in 40 S binding of human eIF3j (8) are *boxed* in *blue*. The *stars below* these regions indicate conserved residue type. *B*, schematic of the eIF3j sequence with the *lines* at the *bottom* depicting the segments of eIF3j used for the eIF3b-RRM interaction studies. *C*, pull-down assays using His-tagged eIF3b-RRM. His-eIF3b-RRM (*lanes 1* and *2*), wild-type eIF3j (*lanes 3* and *4*), Δ16C-eIF3j (*lanes 5* and *6*), Δ69N-eIF3j (*lanes 7* and *8*), and Δ80C-eIF3j (*lanes 9* and *10*) were all tested separately as a control, and the input solution and the elution are shown in *lanes I* and *E*, respectively. The name of the proteins used as input is shown *above* the corresponding *lane* of the gel. *Lane numbers* are shown *below* the gel.

(G196), the first half of helix α1 (Leu[200], Glu[201], Asn[205], and Val[206]), and loop 5 (Leu[255], Asp[256], Gln[258], His[259], and Arg[262]). These perturbed residues map a defined surface opposite from the negatively charged β-sheet area (Fig. 3, *B* and *C*, and supplemental Fig. S3). In accordance, no significant changes are observed for residues located in the RNP sequences (Fig. 3*A*). Interestingly, most of the residues presenting the largest chemical shift perturbations are close to conserved lysine or arginine residues (Fig. 3, *C* and *E*) and thus comprise a conserved positively charged interacting surface. This suggests that electrostatic interactions with this basic surface are important for the recognition and binding of eIF3j to the eIF3b-RRM. This is further supported by the fact that the protein-protein complex is unstable at higher salt concentration (>300 mM NaCl) (data not shown). In addition, we performed a calculation of the evolutionary conservation scores and mapped them on our solution structure by the use of ConSurf (available on the World Wide Web at consurf.tau.ac.il/). We identify that the interacting surface of eIF3j on eIF3b-RRM appears as patches of evolutionarily conserved residues that are spatially close to each other (Fig. 3*D*). This suggests that this region is functionally important and under strong evolutionary constraints, implicating the conservation of the eIF3b-RRM·eIF3j interaction surface in the other species.

The First 69 Amino Acids of eIF3j Are Necessary and Sufficient for Interaction with eIF3b-RRM—Having defined the region of eIF3b-RRM responsible for eIF3j binding, we next sought to identify precisely the recognition site on eIF3j for eIF3b-RRM. The amino acid sequence of eIF3j does not contain any identifiable domain motif or signature. However, there are three regions of eIF3j that are especially interesting as potential candidates for eIF3b-RRM binding (Fig. 4*A*). First, the N terminus of eIF3j contains a cluster of negatively charged residues (residues 43–48 and 53–58), which can potentially complement the positively charged interacting surface of the eIF3b-RRM (Fig. 3*C*). Second, a C-terminal segment spanning residues 210–218 displays homology to the conserved KX_5ERX_2R motif found in yeast homologues of eIF3j (HCR1) and eIF3a (TIF32) (10). This motif in TIF32 is important for the interaction with the yeast eIF3b-RRM, whereas mutation of this motif in HCR1 alters its ability to compensate the defects caused by PRT1 (eIF3b) or TIF32 (eIF3a) mutations (10). Last, the 16 last amino acids of human eIF3j, which have been shown to be important for stable binding to the 40 S ribosomal subunit (8), also contain acidic residues, which can potentially complement the basic interacting surface of eIF3b-RRM.

To identify the interacting subdomain of eIF3j, we designed two C-terminal deletion mutants, in which the last 16 or 80 amino acids were removed (Δ16C-eIF3j and Δ80C-eIF3j) (Fig. 4*B*) and an N-terminal deletion mutant lacking the first 69 amino acids (Δ69N-eIF3j) (Fig. 4*B*). The binding of eIF3j deletion mutants to eIF3b-RRM was tested by pull-down assays using His-tagged eIF3b-RRM (Fig. 4*C*). The mutants lacking

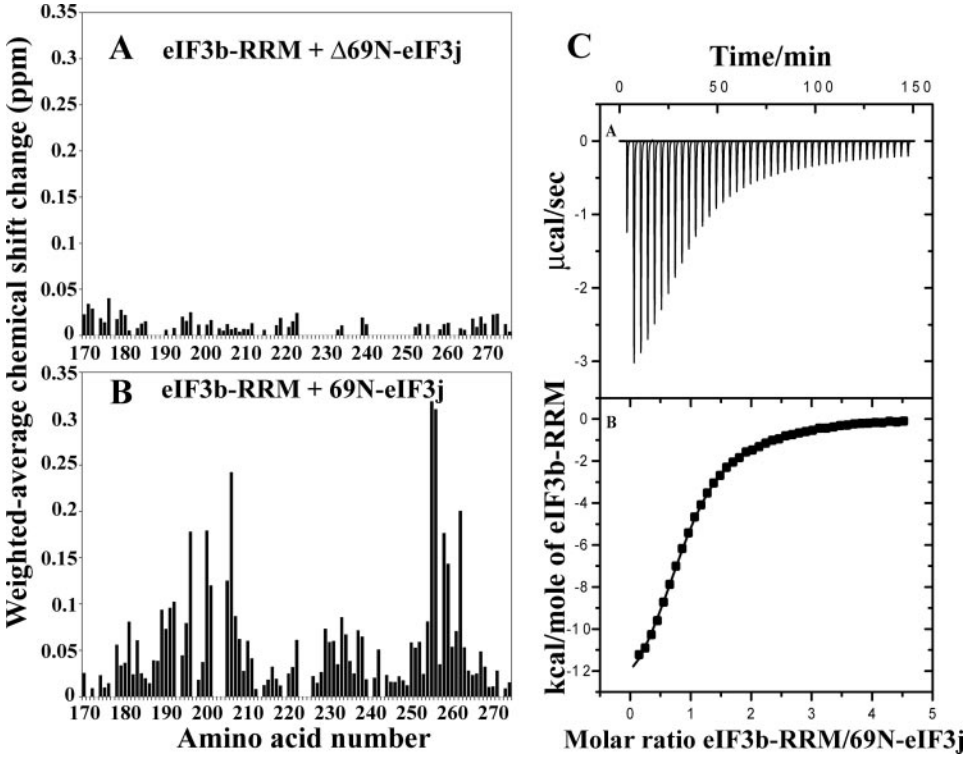

FIGURE 5. **Composite ^{1}H-^{15}N NMR chemical shift changes of the uniformly ^{15}N-labeled eIF3b-RRM observed upon titration of unlabeled Δ69N-eIF3j (*A*) or 69N-eIF3j (*B*).** The amide resonances of 5 residues (Lys^{174}, Arg^{199}, Lys^{202}, Leu^{203}, and Phe^{269}) could not be unambiguously assigned in the bound spectra. *C*, isothermal calorimetric titration of 69N-eIF3j with eIF3b-RRM. The *upper panel* shows the raw ITC thermograms from titration of 7-μl injections of a 1 mM eIF3b-RRM solution into 50 μM 69N-eIF3j. The *lower panel* shows the fitted binding isotherms displaying heat absorbed/released per kcal/mol of eIF3b-RRM injected as a function of molar ratio eIF3b-RRM/69N-eIF3j.

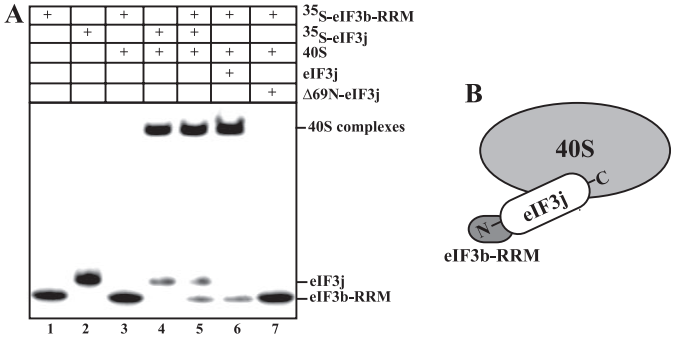

FIGURE 6. *A*, 40 S ribosomal subunit binding assays. Gel mobility shift assay shows the binding of eIF3b-RRM to 40 S ribosomal subunits only when eIF3j is present. The samples corresponding to different combinations of [^{35}S]methionine-labeled or unlabeled proteins incubated or not with 40 S ribosomal proteins (see *table above* the gel) were loaded on a 1% native agarose gel. The labeled proteins were visualized after gel electrophoresis by autoradiography. *B*, schematic of 40 S subunit·eIF3j·eIF3b-RRM complex formation.

the C-terminal parts, Δ16C-eIF3j and Δ80C-eIF3j, were pulled down with the His-tagged eIF3b-RRM as efficiently as the wild-type eIF3j (Fig. 4*C*, *lanes 12* and *14*). On the other hand, the N-terminal deletion mutant, Δ69N-eIF3j, was not pulled down with the His-tagged eIF3b-RRM (Fig. 4*C*, *lane 13*). These results show that the N terminus of eIF3j contains the crucial interacting site between the two proteins and that the C terminus of eIF3j is not involved in the interaction with eIF3b-RRM.

NMR titration experiments were then performed with the eIF3j deletion mutants using uniformly ^{15}N-labeled eIF3b-RRM (Fig. 5 and supplemental Fig. S4). Negligible changes in chemical shifts were observed when Δ69N-eIF3j was added, indicating no appreciable binding when the N terminus is lacking (Fig. 5*A*). In contrast, the addition of Δ16C-eIF3j and Δ80C-eIF3j mutants induced significant chemical shift changes (supplemental Fig. S4). The residues showing the perturbations as well as the magnitude of the displacement were compatible with those seen upon the addition of eIF3j (Fig. 3*A*).

To confirm that the interaction with eIF3b-RRM is mediated by the N terminus of eIF3j, an N-terminal 69-residue fragment was prepared (69N-eIF3j) (Fig. 4*B*). 69N-eIF3j also induced chemical shift changes similar to those seen for wild-type eIF3j (Fig. 5*B*), indicating that the same binding mode is used by eIF3j and 69N-eIF3j to interact with eIF3b-RRM. The thermodynamic parameters characterizing the interaction between 69N-eIF3j and eIF3b-RRM were determined by ITC measurements (Fig. 5*C*). Overall, the binding curve was reminiscent of the one representing the eIF3b-RRM/wild-type eIF3j interaction: a complex stoichiometry of 1:1 and a dissociation constant of 17.0 ± 0.3 μM. Moreover, as with wild-type eIF3j, a high heat release is observed ($\Delta H = -15.0 \pm 0.1$ kcal/mol), suggestive of the involvement of charge-charge interactions in the complex formation. These results prove conclusively that this N-terminal 69-amino acid segment of eIF3j containing a stretch of acidic residues (Fig. 4*A*) presents the residues sufficient and essential to bind the basic interacting surface of eIF3b-RRM (Fig. 3*C*).

Binding of eIF3b-RRM to 40 S Ribosomal Subunits Is Mediated Directly by eIF3j—In humans, eIF3j is not only required for stable recruitment of eIF3 and eIF3 subcomplexes to 40 S subunits but is also capable of binding to 40 S subunits singly (8). So far, we have demonstrated that human eIF3b-RRM and eIF3j form a binary complex (K_d = 20 μM) *in vitro*. We therefore raised the question of whether this interaction is sufficient for the eIF3b-RRM recruitment to the 40 S ribosomal subunit. To test binding of the 40 S subunit to eIF3j and eIF3b-RRM, gel mobility shift assays were performed (Fig. 6). Purified 40 S ribosomal subunits were incubated with each ^{35}S-labeled protein or both. The formation of a binary eIF3j·40 S complex is observed by the appearance of a higher molecular weight band on the native gel, confirming that eIF3j alone can bind to the 40 S subunit *in vitro* (Fig. 6, *lanes 2* and *4*). In contrast, the eIF3b-RRM alone does not form a complex with 40 S subunits (Fig. 6, *lanes 1* and *3*). When stoichiometric amounts of ^{35}S-labeled eIF3j and eIF3b-RRM are incubated with 40 S subunits, the

appearance of the higher molecular weight band is accompanied by the disappearance of free eIF3j and eIF3b-RRM to a similar extent (Fig. 6, *lane 5*). This indicates that both eIF3j and eIF3b-RRM are recruited to the 40 S subunit and that eIF3j is necessary for eIF3b-RRM binding to 40 S ribosome. To provide further evidence that a direct interaction between eIF3j and the eIF3b-RRM is mediating the eIF3b-RRM recruitment to the 40 S subunit, ribosomal complexes were assembled with ^{35}S-labeled eIF3b-RRM and unlabeled eIF3j or Δ69N-eIF3j. In the presence of eIF3j, efficient eIF3b-RRM recruitment to the 40 S subunit is observed (Fig. 6, *lane 6*). By contrast, Δ69N-eIF3j, which does not form a binary complex with the eIF3b-RRM (Figs. 4*C* and 5*A*), fails to recruit the eIF3b-RRM to the 40 S subunit (Fig. 6, *lane 7*). This demonstrates that eIF3j and especially its N terminus directly mediate the recruitment of the eIF3b-RRM to the 40 S ribosomal subunit.

DISCUSSION

eIF3b-RRM Resembles Noncanonical RRMs of the U2AF Homology Motif (UHM) Family—The solution structure of the eIF3b-RRM reveals some features characteristic of a noncanonical RRM. In canonical RRMs, the interaction with the RNA target is usually mediated through specific contacts between the basic and aromatic side chains in the β-sheet area and the RNA bases and backbone (12, 13). The eIF3b-RRM lacks aromatic residues in the RNP2 sequence (see supplemental Fig. S1), and both RNPs are surrounded by acidic residues, rendering the RNA-binding interface in the β-sheet area highly negatively charged (Fig. 1*C*), which is contradictory with RNA recognition and binding. Another noncanonical feature of the eIF3b-RRM is the elongated helix α1, which contains 14 amino acids instead of the 10 residues usually found in canonical RRMs. A noncanonical RRM family has been defined for RRM domains sharing sequence and structural characteristics with U2AF proteins, the UHM family (24). The UHM family is characterized by (i) the absence of aromatic residues in the RNP2 sequence, (ii) an extended highly acidic helix α1, and (iii) the presence of a conserved Arg-*X*-Phe motif in loop 5. The last motif and the negatively charged, extended helix α1 comprise the surface for protein-protein interactions in the UHM family. RNA binding of these RRMs is compromised by the presence of an additional C-terminal helix, which is packed against the β-sheet platform.

Although the eIF3b-RRM seems to be closely related to the UHM family, it differs by several key features: (i) the extended helix α1 is highly basic, (ii) the β-sheet surface is highly negatively charged and not obstructed by a C-terminal helix, and (iii) the eIF3b-RRM does not contain any Arg-*X*-Phe motif. Consistent with the surface charge of its β-sheet area, which prevents a canonical interaction of eIF3b-RRM with RNA, eIF3b-RRM showed no binding to various structured and single-stranded RNAs in gel mobility shift assays (data not shown). Moreover, NMR titration experiments using ^{15}N-labeled eIF3b-RRM and unlabeled single-stranded or double-stranded RNAs did not reveal any specific chemical shift changes in the NMR spectra (data not shown). These observations indicate that the eIF3b-RRM is not an RNA binding module. This is in agreement with previous studies also showing that isolated full-length eIF3b subunit does not bind RNA *in vitro* (7, 26). Additionally, the yeast homologue, which shares 26% identity and 50% similarity with human eIF3b, also fails to bind RNA *in vitro* (27). Within 48 S complexes (28) or in binary internal ribosome entry site RNA·eIF3 complexes (29), RNA binding of mammalian full-length eIF3b has been evidenced by cross-linking to mRNA, indicating that eIF3b can interact with RNA only in the context of eIF3 complexes. Our data suggest that the β-sheet surface of the eIF3b-RRM is an unlikely candidate for mediating the aforementioned RNA cross-links.

The eIF3b-RRM, a Platform for the Interaction with eIF3j—We have shown that the human eIF3b-RRM is not an RNA binding module but instead provides a specific platform for the interaction with human eIF3j (Fig. 2*A*). The eIF3j-interacting surface on the eIF3b-RRM is a positively charged surface spanning from loop 1 to helix α1 and loop 5 (Fig. 3). Our pull-down assays and NMR titration experiments using eIF3j deletion mutants have shown that the eIF3b-RRM binding site of eIF3j resides within its first 69-amino acid segment, which contains stretches of acidic residues (Figs. 4 and 5). The large negative enthalpy of the interaction measured by ITC experiments indicates that this protein-protein interaction is dominated by charge-charge contacts (Figs. 2*B* and 5*C*). The charge complementarity between the positively charged binding surface of the eIF3b-RRM and the acidic residues clustered in the N-terminal region of eIF3j is likely to be the key driving force for this interaction. In accordance, high concentrations of salt disrupted the eIF3b-RRM·eIF3j complex during NMR titration experiments (data not shown). The eIF3j binding to the eIF3 complex displays a similar salt dependence and dissociates from the rest of eIF3 during sucrose density gradient centrifugation in buffer containing 400 mM KCl (28).

Several structures of RRM-protein complexes have been determined previously and showed different recognition modes. Either the binding surface involves their β-sheet surface, thereby competing with canonical RNA binding (30–32), or they use their rear α-helices for protein recognition processes, thus allowing simultaneous binding to RNA (33, 34). For these latter complexes, the protein interaction site of the RRMs mainly involves their helix α1 and the loop 5 region. These protein-protein interactions also serve to enhance RNA binding to the available β-sheet surface of the RRM. In noncanonical RRMs, however, this same mode of protein-protein interactions through the rear α-helices does not result in RNA binding. An example of such an RRM-protein complex is the interaction of U2AF65-RRM3, an RRM from the UHM family (24), with the SF1 ligand peptide (35). In this case, SF1 binding to the RRM occurs through charge-charge interactions with the negatively charged helix α1 and via hydrophobic interactions involving a critical Trp residue in the ligand and a hydrophobic pocket between the α-helices and a conserved Arg-*X*-Phe motif in loop 5. The binding mode between eIF3b-RRM and the N terminus of eIF3j is likely to be very similar to this UHM RRM, since similar secondary structure elements comprise the protein interaction surface (Fig. 3). However, the charges at the protein-protein interaction surface are reversed in the eIF3b-RRM (Fig. 3*C*). The basic interacting surface on the eIF3b-RRM con-

tains a cluster of lysine residues (Fig. 3*E*). These positively charged residues and the other interacting residues identified by NMR define a binding surface that corresponds to the patch of evolutionarily most conserved residues of eIF3b-RRM (Fig. 3*D*). Moreover the acidic amino acid stretches found in the 69 N-terminal amino acids of eIF3j are also conserved in yeast eIF3j (Fig. 4*A*), indicating the probable conservation of this binding mode and recognition between the two proteins.

In both yeast and human eIF3j, this region also contains the only Trp residues (Fig. 4*A*), which are potential candidates for hydrophobic interactions with eIF3b-RRM, similar to the ones found between Trp residue 22 of the SF1 peptide and the Arg-*X*-Phe motif of U2AF65-RRM3 (35, 36). Interestingly, in the case of the eIF3b-RRMs in the same location (loop 5), a consensus His-*X*-Phe sequence exists (from residue 259 to 261) and is part of the binding surface to eIF3j (Fig. 3). Mutagenesis on this motif (H259A/F261A and F261A) abolishes binding to eIF3j (data not shown). We therefore speculate that this His-*X*-Phe motif could potentially mediate a hydrophobic interaction with one of the Trp residues of the N terminus of eIF3j (Fig. 4*A*) as for the U2AF65-RRM3/SF1 interaction (35).

The eIF3j Subunit Mediates Binding of eIF3b-RRM to the 40 S Ribosomal Subunit—In order to perform its multiple roles during initiation of translation, eIF3 needs to bind to 40 S ribosomal subunits. Although eIF3j is a component of a binary eIF3·40 S complex, it is no longer associated with eIF3 and the 40 S subunit in the presence of mRNA as well as in 48 S complexes (4, 28). In such ribosomal particles lacking eIF3j, interactions of eIF3a, eIF3b, and eIF3d with mRNA (28) might then instead support the stable association of eIF3 with the 40 S subunit and thereby replace the requirement of eIF3j for stable eIF3/40 S binding. In addition, the eIF3j subunit is not associated with eIF3 in unactivated T lymphocytes, whereas in activated cells, eIF3j is bound to the eIF3 complex and 40 S ribosomal subunit, resulting in activation of protein synthesis (37). The interaction of eIF3j with eIF3 and the 40 S subunit might therefore also play a role in regulation of protein synthesis in mammalian cells (37).

Studies in yeast propose many contacts between the 40 S subunit and the different yeast eIF3 subunits (3), but stable 40 S subunit binding of eIF3 also requires both the integrity of the RRM of eIF3b as well as the eIF3j subunit (10, 38). Similarly, human eIF3 complex lacking eIF3j and eIF3 subcomplexes consisting of eIF3abgi or only eIF3bgi also require eIF3j to stably associate with 40 S subunits (8, 28). Here we also demonstrate that the isolated eIF3b-RRM requires eIF3j to bind stably to 40 S subunits (Fig. 6, *lanes 5* and *6*). Furthermore, we show that the N-terminal part of eIF3j, which contains the interacting site with the eIF3b-RRM, is required for the recruitment of eIF3b-RRM to the 40 S subunit (Fig. 6, *lane 7*). The C-terminal part of eIF3j is not required for the interaction with eIF3b-RRM (Fig. 4*C* and supplemental Fig. S4) but has been shown to be crucial for the interaction of eIF3j with the 40 S subunit. During apoptosis, a 16-amino acid C-terminal peptide is cleaved by caspase-3 from eIF3j (39), resulting in a truncated protein unable to stably bind the 40 S subunit (8). This indicates that the C-terminal part of eIF3j is required for ribosome binding, whereas we show that its N terminus binds to eIF3b-RRM. Our results suggest a first model in which eIF3j could act as a bridge between the 40 S ribosomal subunit, via its C terminus, and the eIF3 complex, via its N terminus binding to eIF3b-RRM (Fig. 6*B*).

In conclusion, the solution structure of the eIF3b-RRM and the identification of the functional binding mode with the eIF3j subunit provide the first structural insights into the complex network of protein-protein interactions within the eIF3 complex. Understanding the molecular basis of protein-protein interactions between individual eIF3 subunits will provide the structural framework to further dissect their role for eIF3 integrity and 40 S subunit binding and help to unravel the detailed functions of eIF3 subunits during initiation of protein synthesis in eukaryotic cells.

Acknowledgments—We thank Laura Easton for assistance during this work, Ji-Chun Yang for assistance with NMR data collection, and Kiyoshi Nagai and members of his group for stimulating discussions. We thank Oliver Daumke and Wim Vranken for help in ITC measurements and FormatConverter use, respectively.

REFERENCES

1. Pestova, T. V., Kolupaeva, V. G., Lomakin, I. B., Pilipenko, E. V., Shatsky, I. N., Agol, V. I., and Hellen, C. U. (2001) *Proc. Natl. Acad. Sci. U. S. A.* **98,** 7029–7036
2. Mayeur, G. L., Fraser, C. S., Peiretti, F., Block, K. L., and Hershey, J. W. (2003) *Eur. J. Biochem.* **270,** 4133–4139
3. Hinnebusch, A. G. (2006) *Trends Biochem. Sci.* **31,** 553–562
4. Kolupaeva, V. G., Unbehaun, A., Lomakin, I. B., Hellen, C. U., and Pestova, T. V. (2005) *RNA* **11,** 470–486
5. Benne, R., and Hershey, J. W. (1976) *Proc. Natl. Acad. Sci. U. S. A.* **73,** 3005–3009
6. Siridechadilok, B., Fraser, C. S., Hall, R. J., Doudna, J. A., and Nogales, E. (2005) *Science* **310,** 1513–1515
7. Methot, N., Rom, E., Olsen, H., and Sonenberg, N. (1997) *J. Biol. Chem.* **272,** 1110–1116
8. Fraser, C. S., Lee, J. Y., Mayeur, G. L., Bushell, M., Doudna, J. A., and Hershey, J. W. (2004) *J. Biol. Chem.* **279,** 8946–8956
9. Asano, K., Phan, L., Anderson, J., and Hinnebusch, A. G. (1998) *J. Biol. Chem.* **273,** 18573–18585
10. Valasek, L., Phan, L., Schoenfeld, L. W., Valaskova, V., and Hinnebusch, A. G. (2001) *EMBO J.* **20,** 891–904
11. Shalev, A., Valasek, L., Pise-Masison, C. A., Radonovich, M., Phan, L., Clayton, J., He, H., Brady, J. N., Hinnebusch, A. G., and Asano, K. (2001) *J. Biol. Chem.* **276,** 34948–34957
12. Varani, G., and Nagai, K. (1998) *Annu. Rev. Biophys. Biomol. Struct.* **27,** 407–445
13. Maris, C., Dominguez, C., and Allain, F. H. (2005) *FEBS J.* **272,** 2118–2131
14. Goddard, T. D., and Kneller, D. G. (2004) *Sparky*, University of California, San Francisco, CA
15. Cornilescu, G., Delaglio, F., and Bax, A. (1999) *J. Biomol. NMR* **13,** 289–302
16. Guntert, P. (1997) *Methods Mol. Biol.* **60,** 157–194
17. Vranken, W. F., Boucher, W., Stevens, T. J., Fogh, R. H., Pajon, A., Llinas, M., Ulrich, E. L., Markley, J. L., Ionides, J., and Laue, E. D. (2005) *Proteins* **59,** 687–696
18. Brunger, A. T., Adams, P. D., Clore, G. M., DeLano, W. L., Gros, P., Grosse-Kunstleve, R. W., Jiang, J. S., Kuszewski, J., Nilges, M., Pannu, N. S., Read, R. J., Rice, L. M., Simonson, T., and Warren, G. L. (1998) *Acta Crystallogr. Sect. D Biol. Crystallogr.* **54,** 905–921
19. Nederveen, A. J., Doreleijers, J. F., Vranken, W., Miller, Z., Spronk, C. A., Nabuurs, S. B., Guntert, P., Livny, M., Markley, J. L., Nilges, M., Ulrich, E. L., Kaptein, R., and Bonvin, A. M. (2005) *Proteins* **59,** 662–672
20. Laskowski, R. A., Rullmannn, J. A., MacArthur, M. W., Kaptein, R., and

Thornton, J. M. (1996) *J. Biomol. NMR* **8,** 477–486
21. Pestova, T. V., Hellen, C. U., and Shatsky, I. N. (1996) *Mol. Cell Biol.* **16,** 6859–6869
22. Auweter, S. D., Fasan, R., Reymond, L., Underwood, J. G., Black, D. L., Pitsch, S., and Allain, F. H. (2006) *EMBO J.* **25,** 163–173
23. Volpon, L., D'Orso, I., Young, C. R., Frasch, A. C., and Gehring, K. (2005) *Biochemistry* **44,** 3708–3717
24. Kielkopf, C. L., Lucke, S., and Green, M. R. (2004) *Genes Dev.* **18,** 1513–1526
25. Klotz, I. M. (1973) *Ann. N. Y. Acad. Sci.* **226,** 18–35
26. Block, K. L., Vornlocher, H. P., and Hershey, J. W. (1998) *J. Biol. Chem.* **273,** 31901–31908
27. Naranda, T., MacMillan, S. E., and Hershey, J. W. (1994) *J. Biol. Chem.* **269,** 32286–32292
28. Unbehaun, A., Borukhov, S. I., Hellen, C. U., and Pestova, T. V. (2004) *Genes Dev.* **18,** 3078–3093
29. Sizova, D. V., Kolupaeva, V. G., Pestova, T. V., Shatsky, I. N., and Hellen, C. U. (1998) *J. Virol.* **72,** 4775–4782
30. Shi, H., and Xu, R. M. (2003) *Genes Dev.* **17,** 971–976
31. Kadlec, J., Izaurralde, E., and Cusack, S. (2004) *Nat. Struct. Mol. Biol.* **11,** 330–337
32. Schellenberg, M. J., Edwards, R. A., Ritchie, D. B., Kent, O. A., Golas, M. M., Stark, H., Luhrmann, R., Glover, J. N., and MacMillan, A. M. (2006) *Proc. Natl. Acad. Sci. U. S. A.* **103,** 1266–1271
33. Price, S. R., Evans, P. R., and Nagai, K. (1998) *Nature* **394,** 645–650
34. Calero, G., Wilson, K. F., Ly, T., Rios-Steiner, J. L., Clardy, J. C., and Cerione, R. A. (2002) *Nat. Struct. Biol.* **9,** 912–917
35. Selenko, P., Gregorovic, G., Sprangers, R., Stier, G., Rhani, Z., Kramer, A., and Sattler, M. (2003) *Mol. Cell* **11,** 965–976
36. Kielkopf, C. L., Rodionova, N. A., Green, M. R., and Burley, S. K. (2001) *Cell* **106,** 595–605
37. Miyamoto, S., Patel, P., and Hershey, J. W. (2005) *J. Biol. Chem.* **280,** 28251–28264
38. Nielsen, K. H., Valasek, L., Sykes, C., Jivotovskaya, A., and Hinnebusch, A. G. (2006) *Mol. Cell Biol.* **26,** 2984–2998
39. Bushell, M., Wood, W., Clemens, M. J., and Morley, S. J. (2000) *Eur. J. Biochem.* **267,** 1083–1091
40. Koradi, R., Billeter, M., and Wuthrich, K. (1996) *J. Mol. Graph.* **14,** 51–55